Polymer droplets on substrates with striped surface domains: molecular dynamics simulations of equilibrium structure and liquid bridge rupture

2005 J. Phys.: Condens. Matter 17 S4199

(http://iopscience.iop.org/0953-8984/17/49/014)

INSTITUTE OF PHYSICS PUBLISHING JOURNAL OF PHYSICS: CONDENSED MATTER

J. Phys.: Condens. Matter **17** (2005) S4199–S4211 doi:10.1088/0953-8984/17/49/014

Polymer droplets on substrates with striped surface domains: molecular dynamics simulations of equilibrium structure and liquid bridge rupture

Jacqueline Yaneva[1,3], **Andrey Milchev**[1,2] **and Kurt Binder**[2]

[1] Institute for Physical Chemistry, Bulgarian Academy of Sciences, 1113 Sofia, Bulgaria
[2] Johannes-Gutenberg Universität, Institut für Physik, 55099 Mainz, Germany

E-mail: yaneva@ipc.bas.bg

Received 6 July 2005
Published 25 November 2005
Online at stacks.iop.org/JPhysCM/17/S4199

Abstract

The structure of a polymer nanodroplet adsorbed on a flat lyophobic substrate chemically decorated with a lyophilic stripe of width $2R_D$ is studied by molecular dynamics simulation of a coarse-grained bead–spring model of short macromolecules (containing $N = 20$ effective monomers). Varying the stripe width, the strength of the monomer–wall attraction and the temperature, the equilibrium morphology of the resulting droplets is studied and discussed in terms of current phenomenological theories.

In the second part, the behaviour of a liquid bridge connecting two such lyophilic stripes a distance L apart is analysed. It is shown that for large enough L such free-standing films are unstable and rupture, after a hole has nucleated and grown into an elongated cavity in the lateral direction leaving only a cylindrical bridge between the stripes immediately before break-up. The forces acting between the two walls of the slit pore in equilibrium due to the thin film forming the liquid bridge are also estimated as a function of distance between the walls.

(Some figures in this article are in colour only in the electronic version)

1. Introduction

Gaining control of wetting behaviour by using chemically patterned substrates is expected to become a useful technique for various applications. Chemically structured surfaces with lateral patterns of varying wettability can be produced, for instance, by photolithography [1, 2], microcontact printing [3–5], vapour deposition through grids [6], domain formation in Langmuir–Blodgett monolayers [7, 8], electrophoretic colloid assembly [9], lithography with

[3] Author to whom any correspondence should be addressed.

colloid monolayers [10] and microphase separation in diblock copolymer films [11]. Various theoretical considerations [12–21] have predicted very interesting droplet morphologies on such substrates, including also so-called 'morphological wetting transitions' [12, 16, 17]. Most of this work relies on 'macroscopic' theories, i.e. the free energy of a fluid droplet is described by a bulk term proportional to its volume and various surface terms describing the free energy contributions due to the liquid–vapour interface and the liquid–substrate interface(s), or the contact angle, respectively [22–24]. Sometimes a line tension term [25–34] proportional to the length of the three-phase contact line between liquid–vapour and substrate is also included. These macroscopic theories are indeed very useful for the understanding of various phenomena in microfluidics, but one must expect limitations of such theories on the nanoscale [21]. For example, the concepts of a contact line and a contact angle have to be revised, since a sharp contact line is expected to be replaced by a smooth transition from a mesoscopic wetting film to a precursor film which is comparable in thickness to atomic dimensions [34–38]. Also even an atomically sharp boundary between lyophilic and lyophobic areas on the substrate will lead to a smooth lateral variation of the effective interaction potential between the liquid particles and the substrate [35].

A more microscopic description better adapted to such phenomena on the nanoscale is provided by density functional theories [21, 33–39], which are a successful approach to address the static structure on scales intermediate between the macroscopic and the atomistic scales. However, it is the particular merit of molecular dynamics computer simulations [40] that they not only can fully cover phenomena from the atomistic scale to the nanoscale, taking also full account of statistical fluctuations, which are partially ignored in the approaches mentioned above, but also contain important information on the dynamics of the studied model systems. The present technological drive towards nanotechnology, including nanofluidics such as the transport process to and from 'nanoreactors', creates increasing interest in such phenomena.

With this motivation we have recently studied a polymer nanodroplet adsorbed on a circular lyophilic domain on an otherwise lyophobic surface [41]. In the present paper, we treat the related case of nanoscopic polymer droplets adsorbed on a lyophilic stripe (rather than a circular domain). Also the morphology and rupture kinetics of liquid films bridging between two such lyophilic domains in a slit pore of width L will be considered. Whenever possible, we shall make contact with the concepts derived from the related macroscopic theories [12–20] to test their applicability on the nanoscale.

2. Model and simulation technique

Since the phenomena under study require both the consideration of rather large length scales (in the order of up to 100 nm) and related large timescales, it is advisable to consider a coarse-grained model, rather than an atomistic model containing full chemical detail on a particular system [40, 42]. There is ample evidence that the generic properties of melts of flexible polymers can be captured by simple bead–spring models, where each bead may represent a few chemical monomers along the chain backbone [42–46]. Such models take account of chain connectivity and excluded volume interactions between the effective segments, and an attractive interaction between them is also included, which drives the phase separation between the polymer liquid and the gas. Note that, unlike small molecule fluids, the density of polymers in the gas phase can be taken as strictly zero for typical circumstances, and this fact greatly facilitates the simulations (and offsets the disadvantage that density fluctuations relax considerably more slowly in a polymeric liquid rather than a small molecule liquid). Following [44–46] we describe the interactions between the beads modelling the effective

monomeric units by a truncated and shifted Lennard-Jones (LJ) potential,

$$U_{\mathrm{LJ}}(r) = 4\epsilon[(\sigma/r)^{12} - (\sigma/r)^{6}] + 127/4096, \qquad r < 2 \times 2^{1/6}\sigma. \tag{1}$$

Here ϵ describes the strength and σ the range of the LJ potential. It is cut off at twice the minimum distance and shifted so as to produce a continuous potential at this cut-off distance. In addition, monomers along the chain also interact with a finitely extensible nonlinear elastic (FENE) potential,

$$U_{\mathrm{FENE}}(r) = -15\epsilon(R_0/\sigma)^2 \ln(1 - r^2/R_0^2), \qquad R_0 = 1.5\sigma. \tag{2}$$

The choice of these parameters ensures that the minimum of the total potential between two bonded monomers along the chain occurs for $r \approx 0.96\sigma$, while the minimum of the LJ potential between non-bonded monomers occurs for $r = 2^{1/6}\sigma \approx 1.126$, of course. The misfit between these two distances ensures that no crystallization occurs there, on timescales accessible by MD, and rather at low temperatures ($T/\epsilon \approx 0.4$) a glass transition of dense melts is found in the bulk [44, 45]. Henceforth we shall measure all lengths in units of σ and all energies (including the temperature, choosing $k_{\mathrm{B}} = 1$) in units of ϵ. The chain length is chosen as $N = 20$ throughout. Since the Theta-temperature of this model (i.e., the limit of the gas–liquid critical temperatures for $N \to \infty$) is known to occur for about $T_0 \approx 3.1$, it is possible to work in a temperature range $0.6 \leqslant T \leqslant 1.0$ where the system is not yet slowed down by the glass transition but nevertheless the density of the monomers in the gas is still indistinguishable from zero. In this respect, a somewhat wider range of temperatures is accessible with the present model rather than with the related model [41–43] that was used in our previous work on droplets on circular lyophilic domains [41]. In addition, the present model allows us to use a somewhat larger molecular dynamics (MD) time step, namely $\delta t = 0.005$ MD time units rather than [41] $\delta t = 0.0009$ MD time units, and hence no efficiency is lost in spite of the larger range of the present potential.

The adsorbing walls are treated as perfectly flat and structureless; in particular, no atomic corrugation of the walls is considered. The interactions between the effective monomers and the walls are represented by a Lennard-Jones potential that is integrated over a semi-infinite substrate

$$U_{\mathrm{wall}}(\Delta z) = \epsilon_{\mathrm{w}}[(\sigma_{\mathrm{wall}}/\Delta z)^9 - (\sigma_{\mathrm{wall}}/\Delta z)^3], \tag{3}$$

Δz being the distance from the substrate. We choose parameters $\sigma_{\mathrm{wall}} = 1$, $\epsilon_{\mathrm{w}} = 0.05$ in the lyophobic part. Thus, we ignore the effect that $U_{\mathrm{wall}}(\Delta z)$ should be smooth at the boundary between lyophobic and lyophilic regions [35] and that for a lyophilic strip of finite width a faster decay than described by equation (3) is expected.

Typically the size of the simulation box is chosen to be $L_x \times L_y \times L_z = 64 \times 76 \times 40$, the lyophobic substrate being at $z = -20$. The lyophilic area is modelled as a band along the whole distance L_y which has a width $2R_D$, with $3 \leqslant R_D \leqslant 18$. The total number of chains in the polymer droplet is chosen as $\mathcal{N} = 512$ (for a sessile droplet) and $\mathcal{N} = 1024$ (for a bridging droplet). Periodic boundary conditions are implemented in the x and y directions, so the droplet (which often is rather elongated in the y-direction) can interact with its periodic images in that direction and in the extreme case it can form a continuous liquid stripe in that direction. Since we put the droplet in the middle of the lyophilic area, so its x-coordinate is $-R_D \leqslant x \leqslant R_D$, the periodic boundary condition in the x-direction only has the effect that chains that evaporate from the droplet (this occasionally happens for temperatures $T > 1$) and leave the box in the x-direction will re-enter from the $-x$ side, and vice versa. The top wall of the box, at $z = 20$, is taken to be purely repulsive (if a monomer reaches this wall then the monomer velocity changes its sign, thus preventing chains from leaving the simulation box). If we wish to simulate liquid bridges, the same potential equation (3) is applied at both walls.

Our simulations are run at temperatures from $T = 0.6$ (where the number density in the liquid phase at zero pressure is $\phi \approx 0.9$) up to $T = 1.4$ (where $\phi = 0.6$). While at $T < 1.1$ there is no evaporation occurring and the gas density is zero, to a very good approximation, already at $T \geqslant 1.1$ some evaporation events of chains from the interface of the model were observed. For $T \geqslant 1.4$ the droplet is found to be rather unstable; many chains can evaporate.

For our study of slit pores, we use distances L between the walls in the range $8 \leqslant L \leqslant 52$. The initial preparation of droplets in equilibrium is done by Monte Carlo methods, as described elsewhere [41]. MD runs are performed applying the standard velocity Verlet algorithm [40] and the temperature is kept constant via the Langevin thermostat [40], which provides a very good stability of the algorithm. The coordinate of each monomer then changes according to

$$m\ddot{\vec{r}}_i = \vec{F}_i - \xi(\Delta z)\dot{\vec{r}}_i + W_i(t), \tag{4}$$

where $m = 1$ is the mass of an effective monomer and $\vec{F}_i$ is the force deriving from all the potentials

$$\vec{F}_i = -\sum_{j(\neq i)} \partial U_{ij}/\partial \vec{r}_i, \qquad U_{ij} = U_{ij}^{\mathrm{LJ}} + U_{ij}^{\mathrm{FENE}} + U_{ij}^{\mathrm{wall}}. \tag{5}$$

$\vec{W}_i(t)$ is a Gaussian white noise term,

$$\langle \vec{W}_i(t) \cdot \vec{W}_j(t') \rangle = 6Tm\xi\delta_{ij}\delta(t - t'). \tag{6}$$

Note that we use the thermostat near the wall only,

$$\xi(\Delta z) = \xi^* \exp(\sigma - \Delta z), \qquad \xi^* = 15, \tag{7}$$

motivated by the idea that physically equilibration is achieved via heat transport to and from the wall. Typically one run is over 1.1 million integration time steps.

3. Polymer nanodroplets on stripe-like domains

In their pioneering study on wetting morphologies on substrates with striped surface domains, Brinkmann and Lipowsky [18] proposed to use the contact angle of the lyophilic domain Θ_{phil} and the reduced volume of the liquid phase $q = V/(2R_D)^3$ as the basic control parameters (while the contact angle of the lyophobic domain was typically put at its limiting value $\Theta_{\mathrm{phob}} = \pi$, and line tension effects were neglected). Brinkmann and Lipowsky [18] consider four morphologies: (I) small spherical cap (for small enough q); (II) extended channel (for large q but large enough Θ_{phil}); (III) droplike state with contact line pinned to the boundary of the surface stripe (for large q and sufficiently small Θ_{phil}); (IV) droplike state with contact line depinned from the boundary of the surface stripe (for large q and sufficiently small Θ_{phil} but $\Theta_{\mathrm{phob}} < \pi$). Studying the stability of states I, II, and III for $\Theta_{\mathrm{phob}} = \pi$ in the framework of their 'macroscopic theory', Brinkmann and Lipowsky [18] find that the change from I to III is a discontinuous transition along a line in the plane (q, Θ_{phil}). This line (as well as the associated limits of metastability) ends in a kind of critical point at $q_{\mathrm{crit}} \approx 2.85$, $\Theta_{\mathrm{phil}}^{\mathrm{crit}} \approx 39.2$. For $\Theta_{\mathrm{phil}} > \Theta_{\mathrm{phil}}^{\mathrm{crit}}$, one encounters only a smooth change from state I to state III.

Turning now to our simulations, it is straightforward to vary the parameter q simply by suitably changing the stripe width $2R_D$. It is a nontrivial issue to ensure that the contact angle Θ_{phil} occurs in the range of interest. We can vary Θ_{phil} by either changing the strength of the substrate potential ϵ_{w}, equation (3), or by changing the temperature T; note that the liquid–gas surface tension $\gamma_{\ell\mathrm{g}}$ of the polymer melt shows a rather strong decrease with increasing temperature (it vanishes at the gas–liquid transition temperature $T_{\mathrm{c}}(N)$), while the polymer–substrate surface tension $\gamma_{\ell\mathrm{w}}$ is approximately proportional to ϵ_{w} since in the regime of interest the polymer density in the gas phase is negligibly small, the corresponding surface

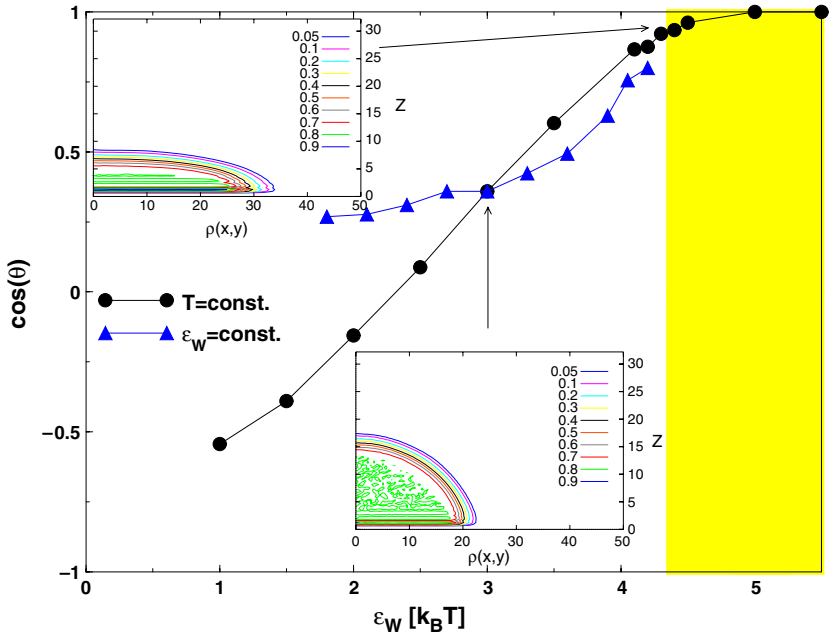

Figure 1. Cosine of the contact angle of a polymer droplet containing $N_{ch} = 512$ chains of length $N = 20$ on a uniform flat substrate at which the wall potential, specified by equation (3), acts, plotted versus ϵ_w at $T = 1.0$ (full circles). Triangles show corresponding data plotted versus T ($T = 0.6, 0.7, 0.8, 0.9, 1.0, 1.1, 1.2, 1.3, 1.4, 1.5$, from left to right) at $\epsilon_w = 3$. In the shaded region the substrate is wet. Insets show for two typical cases the contour diagrams that describe the density profiles of the droplets. For further explanations cf text.

tension γ_{gw} vanishes, and hence the Young equation for the contact angle [22] simply reads $\gamma_{\ell g} \cos\Theta = \gamma_{\ell w} - \gamma_{gw} = \gamma_{\ell w}$. Thus we expect that at constant $\gamma_{\ell g}$ (i.e. constant temperature) the cosine of the contact angle varies roughly linearly with ϵ_w. Figure 1 shows MD results that confirm our expectation. Following previous studies of a related model [47], polymer droplets are prepared on a uniform surface (without a stripe domain) with a chosen value of ϵ_w in equation (3) and equilibrated to record the density distribution $\rho(r, z)$ of the droplet, where the z-axis is chosen perpendicular to the substrate surface through the centre of mass of the droplet, and r is a radial coordinate measured from this axis. The insets in figure 1 show typical examples of such density distributions, showing contours $\rho(r, z) = 0.05, 0.1, 0.2, \ldots, 0.9$ as indicated. The midpoint contour $\rho(r, z) = 0.4$ is used to estimate the contact angle Θ by fitting a straight line to this contour in the region $2 \leqslant z \leqslant 4$. Of course, due to the smallness of the droplet there is no straight line portion present in the contours $\rho(r, z) =$ constant at all, rather some curvature is inevitably present, and thus only tentative estimates of $\cos\Theta$ can be obtained, subject to some systematic error. An alternative method would be [47] the estimation of $\gamma_{\ell w}$, $\gamma_{\ell g}$ for a flat ultrathin film with horizontal interfaces, using then the Young equation to obtain $\cos\Theta$. However, on the nanoscale one must expect substantial deviations from the Young equation due to line tension effects [47, 48] and thus it is not clear that this method should be preferred. It is also clear that for small droplets the transition from nonwet to wet surfaces ($\cos\Theta \to 1$) is somewhat rounded, but it is plausible to assume that $\epsilon_w = 4.5$ refers already to a wet state of the surface, for $T = 1.0$, while $\epsilon_w = 3.0$ corresponds to $\cos(\Theta) \approx 0.35$ and hence $\Theta_{phil} \approx 70$ or thereabout. Even if one accepts very generous error

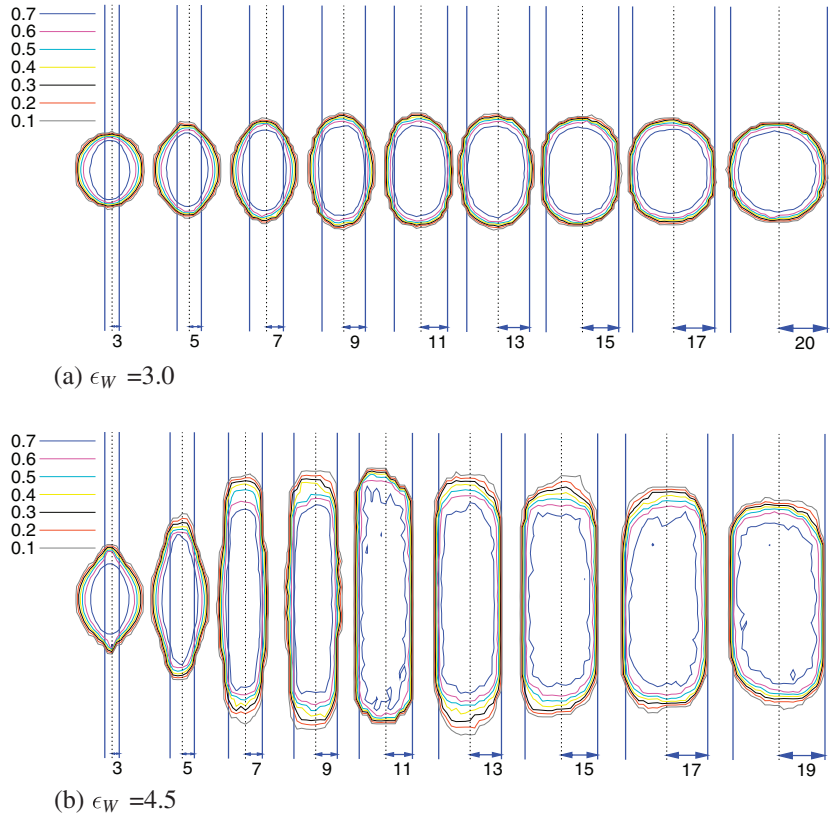

Figure 2. Projections of the density distributions of polymer droplets on lyophilic stripes on the surface plane, for stripe halfwidths $R_D = 3, 5, 7, 9, 11, 13, 15, 17$, and 20 and the choice $T = 1, \epsilon_w = 3.0$ (a) and for the choice $T = 1, \epsilon_w = 4.5$ (b). Curves show contours of constant density $\rho(x, y) = 0.1, 0.2, 0.3, 0.4, 0.5, 0.6$, and 0.7, as indicated. Droplets contain 512 chains of length $N = 20$ throughout, and hence their volume is always the same. Thus for small R_D the height of the droplets in the z-direction normal to the substrate plane (this height is not displayed here) is much larger than for large R_D. Outside of the lyophilic stripe $\epsilon_w = 0.05$ which provides $\Theta_{phob} \sim \pi$ and then the contact line always stays pinned to the stripe boundaries.

bars to this estimate, it is clear that for $\epsilon_w = 3.0$ we are far above the critical value Θ^{crit}_{phil} of Brinkmann and Lipowsky [18], and hence we expect a gradual transition from a sphere-cap shaped droplet (state I) for large R_D (i.e., small q) to a droplike state with contact line pinned to the surface domain boundary (state III).

Figure 2 shows that for $\epsilon_w = 3.0$ and for large R_D (i.e., small q) the droplet indeed has a spherical shape, whereas when R_D decreases, and q hence increases, the droplet shape is elongated along the stripe axis. The whole droplet stays on the stripe for $R_D \geqslant 15$, while for $R_D \leqslant 13$ part of the liquid goes out of the stripe. For $R_D \leqslant 7$ it is evident that the part of the droplet that is not close to the stripe tends to return to a spherical surface, and thus contours for the different values of density no longer have the same shape: e.g., for $R_D = 3$ the contour $\rho(x, y) = 0.7$ (this is the innermost contour; in the z-direction it is closest to the substrate) clearly has a shape close to elliptic shape, while contours for small density have almost spherical shape. As expected for such small droplets, the change of the droplet shape with stripe width is not a discontinuous process but a gradual, rounded transition.

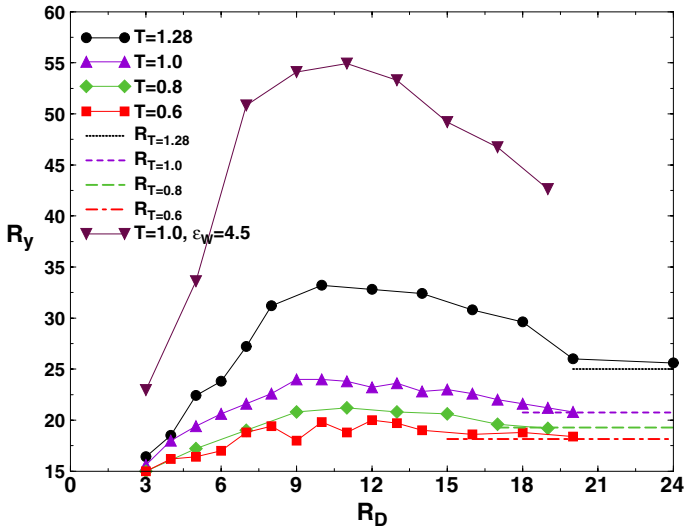

Figure 3. Plot of the half linear dimension (R_y is the droplet radius if their shape is sphere-cap-like) versus the halfwidth R_D of the lyophilic stripes at four temperatures, as indicated in the figure. The broken horizontal straight lines show the asymptotic values derived from droplets on surfaces which do not have a lyophobic surface domain at all. Data for a 'wet' stripe (with $\epsilon_w = 4.5$) are also included (here no asymptote can be shown due to complete spreading of a droplet on a surface without lyophobic domain).

For $\epsilon_w = 4.5$, where we expect zero contact angle in the thermodynamic limit, we observe elongated extended channel states for all $R_D \geqslant 11$, and the contact line seems to be perfectly pinned along the surface domain boundaries. For smaller R_D, however, a part of the droplet starts to make excursions into the hydrophobic region, and for $R_D = 5$ and 3, we indeed have a morphology of an elongated droplet, with a pinned contact line (i.e., type III in the Brinkmann–Lipowsky [18] classification). Indeed, the transition into a droplet shape from an elongated cigar for $R_D = 7$ to a deformed ellipsoid for $R_D = 5$ is much more abrupt than the corresponding changes for $\epsilon_w = 3$; probably one can interpret this rather rapid change of morphology with R_D for $\epsilon_w = 4.5$ as a remnant of the first order transition from topology II to topology III or IV, rounded by finite size.

To quantify these observations a bit more we study the dependence of the droplet linear dimension in the direction of the stripes (the y-direction) as a function of R_D, varying the temperature for $\epsilon_w = 3.0$ (figure 3). In all cases the maximum of this non-monotonic variation of R_y with R_D occurs for $R_D \approx 10$. However, we do not expect that a quantitative comparison with the macroscopic theory of Brinkmann and Lipowsky [18] would make much sense as line tension effects, statistical fluctuations, effects due to molecular structure, etc, are all ignored in their treatment; one cannot expect a quantitative accuracy on the nanoscale. Therefore, it is rather involved to obtain information such as that shown in figure 3 from this macroscopic theory, and we have not attempted to do this.

Finally in this section we turn to cylindrical droplets (with twice as many chains, $\mathcal{N} = 1024$) confined between two walls with lyophilic stripes (of halfwidth $R_D = 18$) exactly opposite each other, varying their distance L, and studying the relation between the force versus L curve and the shape of the resulting polymer film bridging between the plates. For too small a separation the polymers do not fit completely on the lyophilic parts of the surfaces, and are somewhat squeezed out into the lyophobic part, resulting then in a convex

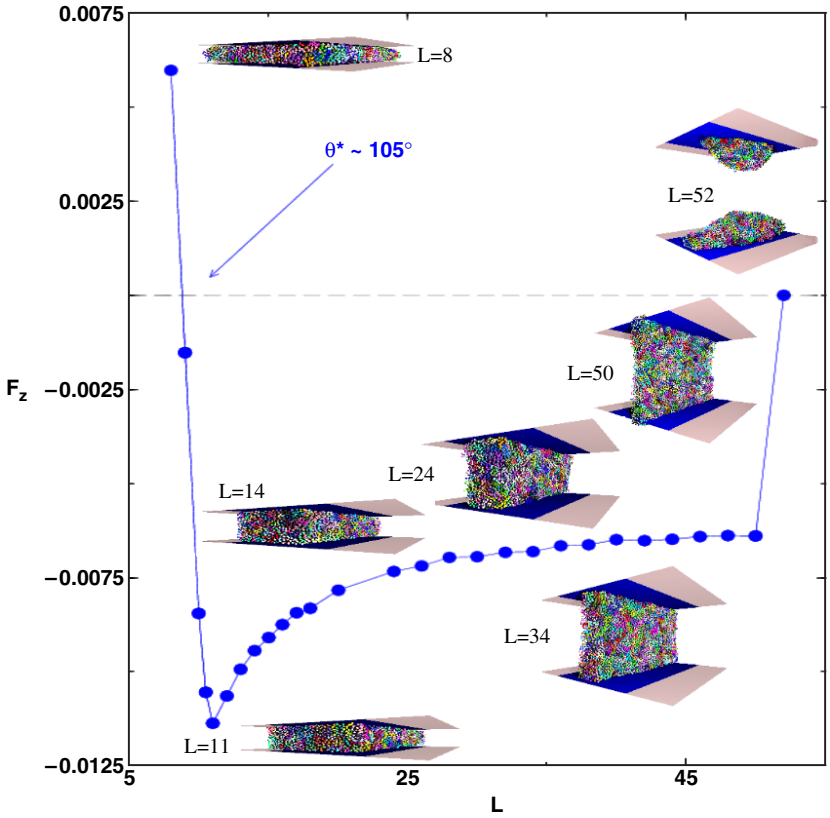

Figure 4. Force between two surfaces containing lyophilic stripes of halfwidth $R_D = 18$ exactly opposite each other, with a polymer film containing $\mathcal{N} = 1024$ chains of length $N = 20$ adsorbed on both stripes connecting them, plotted versus their separation L. For some selected cases snapshots of the film are shown (note that for $L = 52$ the film has ruptured into two disconnected droplets, and thus the force ceases to exist). The lyophilic parts of the surfaces are shown in black, lyophobic parts in grey. All data refer to $T = 0.6$, every point is obtained by averaging over three independent runs of 0.5 million MD steps, and $\epsilon_w = 3.0$.

(outbound) polymer–gas interface, and a repulsive force ($F_s > 0$). For $L = 11$ the polymer film fits perfectly to the lyophilic stripes, and the polymer–gas interface is perfectly horizontal, connecting both the upper and the lower contact lines. Here the F_z versus L curve has a rather steep minimum, corresponding to the strongest attraction (no force occurs when the contact angle is not 90° but roughly 105°). As L increases further, the forces stay attractive (negative) while the liquid–gas interfaces of the polymer film become slightly concave (inward bound), and a smaller and smaller part of the lyophilic stripe is still covered with polymers, until at $L = 52$ the film becomes unstable and ruptures, so the system takes states of the type shown in figure 4. The kinetics of this rupture process of such free-standing thin polymer films suspended between attractive stripes at walls will be analysed in the next section.

4. Kinetics of thin film rupture

In this section we study the break-up of a thin polymer film which forms a free-standing liquid bridge between the two lyophilic stripes opposite each other on the otherwise lyophobic

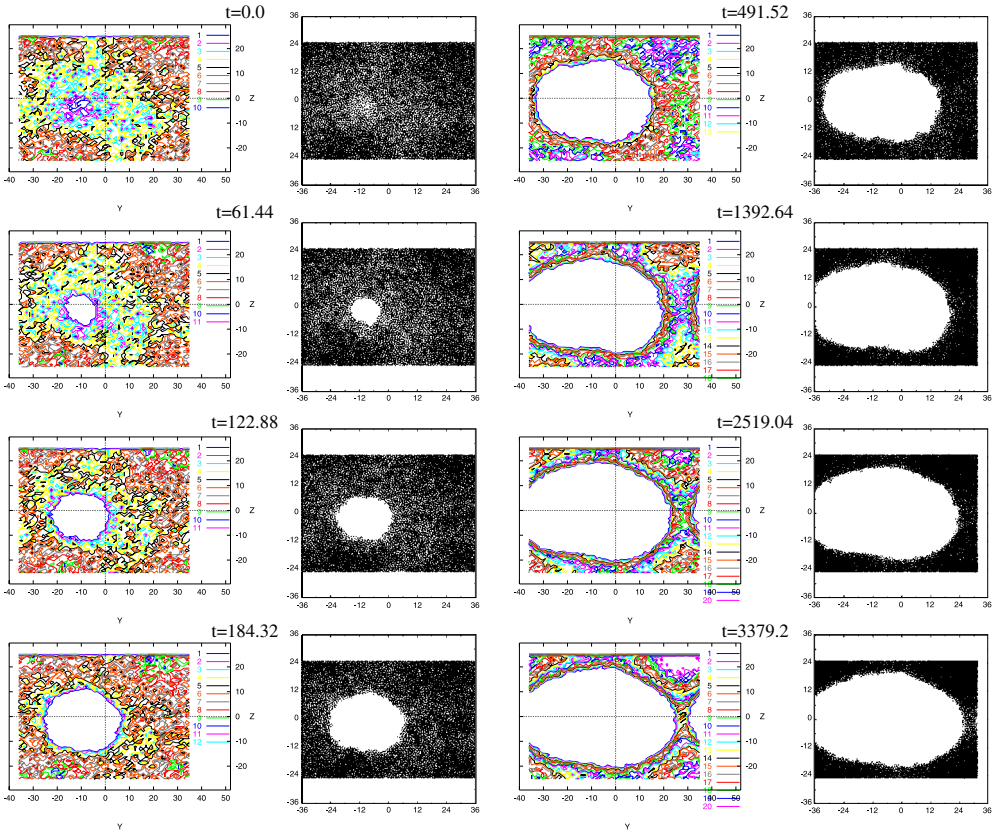

Figure 5. Snapshot pictures of the time evolution (time is measured in the standard MD time units) of a thin film between two lyophilic stripes at distance $L = 52$ from each other in the z-direction, while in the y-direction periodic boundary conditions are used, for the choice of parameters $T = 0.6$, $\epsilon_w = 3.0$; $\mathcal{N} = 1024$, $N = 20$. The left series of pictures shows contours of the local film thickness in columns of cross sections $\Delta y \times \Delta z$ in the x-direction parallel to the walls (that is, the xy-planes at $z = -26$ and +26, respectively). The right series of pictures were generated simply by projecting the y, z-coordinates of each monomer in the film onto one yz-plane. Both columns on the left show the early time evolution, namely times $t = 0.0$, 61.44, 122.88, and 184.32, while the other two columns on the right show the late time evolution ($t = 491.52$, 1392.64, 2519.04, and 3379.2, respectively).

surfaces in more detail. Figures 5(a) and (b) present a series of snapshot pictures which attempt to visualize the kinetics of these phenomena by suitable projections into a plane parallel to the free surface of the thin film.

Since the gas–liquid interfaces of the thin film are slightly concave, the thickness of the film is smallest near $z = 0$. Given the fact that the interfaces must exhibit some thermal capillary wave-type fluctuations, it then is possible to find a spot near $z = 0$ and some y-coordinate where the barrier against nucleation of a hole in the film is so small that a hole is formed almost immediately after the system is prepared in the considered state. Figure 5(a) shows that this hole starts out with a cross section close to circular but rather soon develops an elliptical shape: obviously hole growth is easier near $z = 0$ in the y-direction rather than close to the walls with the lyophilic stripes. The area taken by the projection of the hole into the yz-plane steadily grows, and at times of order $t = 1000$ the area of the hole starts to exceed

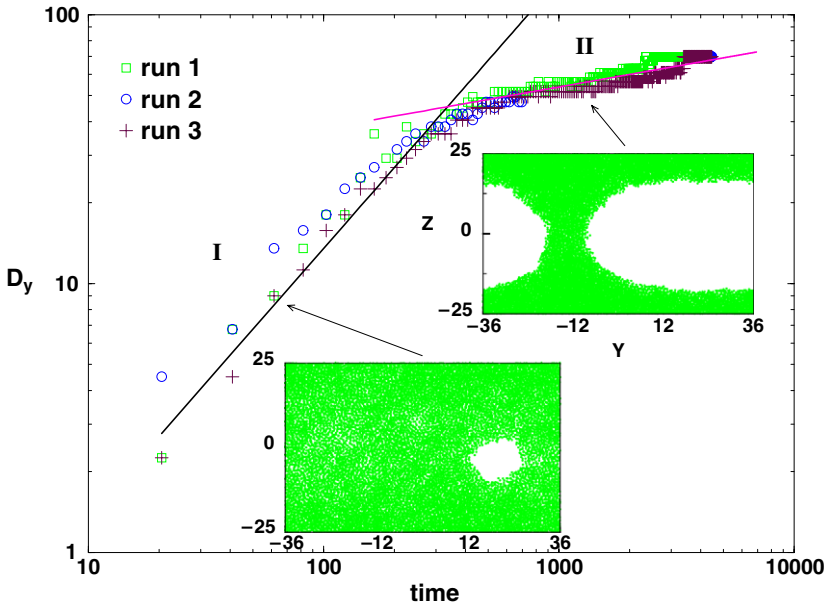

Figure 6. Hole diameter D_y plotted versus time, for the same parameters as shown in figure 5. Three equivalent runs are included. Straight lines on the log–log plot illustrate power laws $D_y \propto t$ in regime I and $D_y \propto t^{0.15}$ in regime II, respectively.

the area still taken by the projection of the liquid film. Actually, at times $t \geqslant 1500$ almost all monomers are now in elongated domains attached to the two lyophilic stripes, and all that is left from the thin liquid film spanning the whole distance $L = 52$ between the two stripes is a thin liquid bridge, which ruptures in the example shown in figure 5 soon after the last snapshot shown.

Figure 6 presents the time evolution of the hole diameter of the rupturing film on a log–log plot. The linear growth of the hole diameter with time, $D_y \propto t$, that is observed until $t \approx 300$ MD units, differs markedly from the exponential growth of hole sizes with time in freely suspended thin viscous films proposed by Debregéas *et al* [49] and from the growth laws discussed for spinodal dewetting of supported thin films (see [50] for references). Of course, the free-standing polymer films whose rupture is considered in the literature [49, 51] have macroscopic rather than nanoscopic lateral dimensions. During the stage where the hole in such films grows exponentially with time the thickness of the remaining film stays constant everywhere. However, in our case the film thickness is distinctly nonuniform, due to the concave shape of the cross section through the film (cf also figure 4). In fact, we observe that the film thickness is about $W \approx 10$ near the walls but only about $W \approx 5$ near $z = L/2$. Studying the flow of material in a viscous liquid film with such inhomogeneous linear dimensions from a hole to the walls is a complicated problem of hydrodynamics that we are not going to address here. Similarly, in the late stages of hole growth (region II in figure 6) mass has to be transported from the centre of the liquid bridge (at $z = 0$) to the regions near the walls, and there the excess mass contained in the conical 'feet' of the liquid bridge has to spread sideways into the positive or negative y-direction along the elongated liquid channel. This spreading of liquid material is somewhat reminiscent of the spreading of liquid droplets on wet substrates (see [52, 53] for references).

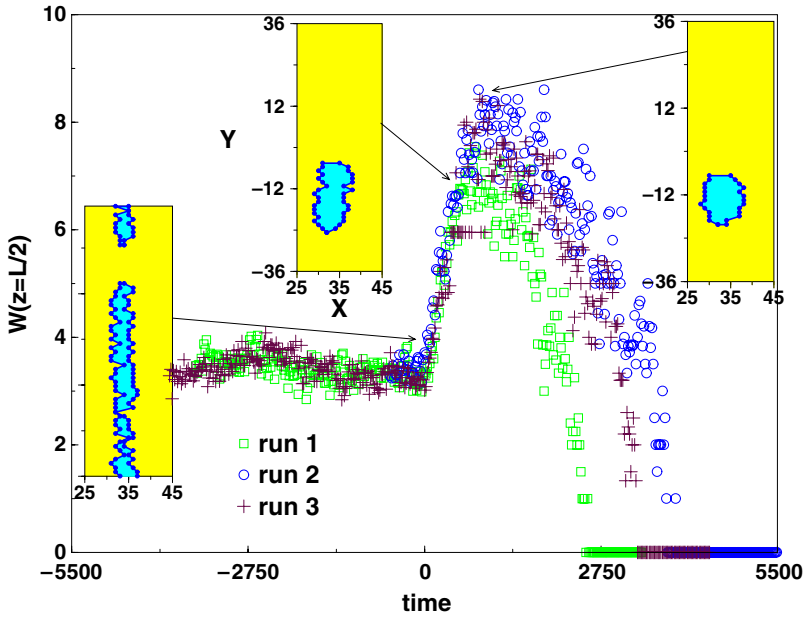

Figure 7. Time evolution of the mid-height film thickness W, for the same set of parameters as in figure 5. At three times characteristic cross-sections of the film at $z = L/2$ in x, y-directions are included. Three equivalent runs are shown.

A further interesting observation concerns the time evolution of the film thickness W at the mid-height (i.e., $z = L/2$) of the film. This quantity is fluctuating around a constant ($z \approx 3.5$) as long as hole nucleation has not yet started (negative times in figure 7: in each run we choose $t = 0$ at the time where hole formation starts). When hole formation has started, the film thickness grows, so the mass from the growing hole stays first at $z = L/2$ (at least to a large extent), leading to a thickening of the remaining film. When the liquid bridge has transformed its elliptical cross section into a circular cross section (at about $t = 10^3$), the maximum thickness of about $W(z = L/2) = 8.5$ is reached (figure 7). Then the thickness decreases until at $W(z = L/2) \approx 1$ the final rupture occurs. Note that in this final stage there is a considerable fluctuation from run to run, unlike the earlier stages. We also note that the crossover characterized by the maximum of $W(z = L/2)$ does correspond to the crossover in the growth law for the hole diameter (figure 6). It hence remains a challenge to theory to correlate all these observations from simulation.

5. Conclusions

Motivated by the work of Lipowsky *et al* [12–20], we have studied in the present work nanoscopic fluid droplets both on isolated lyophilic stripes on otherwise lyophobic substrates, and ultrathin polymer films held between two such stripes on surfaces a small distance L apart. Unlike the macroscopic theory [12–20] which neglects statistical fluctuations due to its mean-field type character, but which also disregards line tension contributions as well as any effects on the atomistic scale (e.g. due to the packing of the molecules at a flat substrate, etc), our MD simulations of a coarse-grained model of short flexible polymer chains in principle include all such effects and hence can provide a check on to what extent the macroscopic theory still

can account for such phenomena at the nanoscale. As expected on general grounds [21], we have found that the transitions between various droplet morphologies are rather gradual on the nanoscale; no evidence for a sharp first-order-like phase transition with associated hysteresis was seen. Of course, such sharp phase transitions in nanoscopically small systems are rounded off by finite-size effects, but apart from this lack of sharp morphological phase transitions in the droplet shapes we find that the macroscopic theory still is rather useful for a qualitative understanding of the observed equilibrium behaviour.

We have also reported some first observations on the kinetics of thin film rupture through the nucleation and growth of holes in ultrathin polymer films held as free standing objects between two lyophilic stripes at two surfaces a distance L apart. Due to the inhomogeneous structure of such films (their thickness near the walls exceeds the film thickness $W(z = L/2)$ at film mid-height distinctly), a description of the kinetics of rupture in such films clearly is difficult, and not attempted in our work (and we are not aware of theoretical work of other groups dealing with this problem). Thus providing a theoretical understanding of our observations, namely a first stage of hole growth where the hole radius varies linearly with time, followed by a second much slower stage where the remaining liquid bridge with roughly circular cross section gets thinner and thinner, and the accompanying changes of the film thickness, figure 7, remains a challenge for the future.

Of course, the present modelling can be viewed as a modest first step only, and many interesting aspects had to be disregarded. Thus, our coarse-grained polymer model disregards effects of chain stiffness, and even on a coarse-grained level is suitable for neutral polymers only. Also the substrate was strongly idealized (perfectly flat and ideal, no atomistic corrugation or mesoscopic roughness, etc). We also emphasize that the choice made to consider very short chains ($N = 20$) excludes any effects specific for the dynamics of long polymers (such as reptation [54]), which may affect the macroscopic growth laws as well. We do hope that the present work will stimulate both further theoretical and experimental studies of these interesting problems.

Acknowledgment

This research was supported in part by the Deutsche Forschungsgemeinschaft (DFG) under grant number 436 BUL 113/130.

References

[1] Wang R *et al* 1998 *Nature* **388** 431
[2] Möller G, Hake M and Motschmann H 1998 *Langmuir* **14** 4955
[3] Lopez G P, Biebuyck H A, Frisbie C D and Whitesides G M 1993 *Science* **260** 647
[4] Drelich J, Miller J D, Kumar A and Whitesides G M 1994 *Colloids Surf.* A **93** 1
[5] Morhand F, Schumacher J, Lenenbach A, Wilhelm T, Dahint R, Grunze M and Everhart D S 1997 *Electrochem. Soc. Proc.* **97** 1058
[6] Gau H, Herminghaus S, Lenz P and Lipowsky R 1999 *Science* **283** 46
[7] Wang R, Parckh A N, Beers J D, Shreve A P and Swanson B 1999 *J. Phys. Chem.* B **103** 10149
[8] Gleiche M, Chis L F and Frecks H 2000 *Nature* **403** 173
[9] Hayward R C, Saville A D and Akroy I A 2000 *Nature* **404** 56
[10] Burmeister F, Schäfte C, Matthews T, Böhmisch M, Boneberg J and Leiderer P 1997 *Langmuir* **13** 2983
[11] Heier J, Kramer E J, Walheim S and Krausch G 1997 *Macromolecules* **30** 6610
[12] Lenz P and Liposwky R 2000 *Phys. Rev. Lett.* **80** 1920
[13] Lipowsky R, Lenz P and Swain P S 2000 *Colloids Surf.* A **61** 3
[14] Swain P S and Lipowsky R 2001 *Langmuir* **17** 23390
[15] Valencia A, Brinkmann M and Lipowsky R 2001 *Langmuir* **17** 3390

[16] Lipowsky R 2001 *Curr. Opin. Colloid Interface Sci.* **6** 40
[17] Lipowsky R 2001 *Interface Sci.* **9** 105
[18] Brinkmann M and Lipowsky R 2002 *J. Appl. Phys.* **92** 4296
[19] Brinkmann M, Kürfeld J and Lipowsky R 2004 *J. Phys. A: Math. Gen.* **37** 11547
[20] Lipowsky R, Brinkmann M, Dimova R, Franke T, Kürfeld J and Zhang X 2005 *J. Phys.: Condens. Matter* **17** S537
[21] Dietrich S, Popescu M N and Rauscher M 2005 *J. Phys.: Condens. Matter* **17** S577
[22] Young T 1805 *Phil. Trans. R. Soc.* **5** 65
[23] Rowlinson J S and Widom B 1982 *Molecular Theory of Capillarity* (Oxford: Clarendon)
[24] De Gennes P G 1985 *Rev. Mod. Phys.* **57** 825
[25] Berry M V 1985 *J. Phys. A: Math. Gen.* **7** 231
[26] Pethica B A 1977 *J. Colloid Interface Sci.* **62** 569
[27] Tarazona P and Navascués G 1992 *J. Chem. Phys.* **75** 925
[28] Toshev B V, Platikanow D and Scheludko A 1988 *Langmuir* **4** 489
[29] Szleifer I and Widom B 1992 *Mol. Phys.* **75** 925
[30] Varea C and Robledo A 1992 *Physica* A **183** 121
[31] Drelich J 1996 *Colloids Surf.* A **116** 43
[32] Bresme F and Quirke N 1998 *Phys. Rev. Lett.* **80** 3791
[33] Getta T and Dietrich S 1998 *Phys. Ref.* E **57** 655
[34] Bauer C and Dietrich S 1999 *Eur. Phys. J.* B **10** 767
[35] Koch W, Dietrich S and Napiórkowski M 1995 *Phys. Rev.* E **51** 3300
[36] Bauer C and Dietrich S 1998 *Phys. Rev.* E **60** 6919
[37] Bauer C, Dietrich S and Parry A O 1999 *Europhys. Lett.* **47** 474
[38] Bauer C and Dietrich S 2000 *Phys. Rev.* E **61** 1664
[39] Dietrich S 1999 *New Approaches to Old and New Problems in Liquid State Theory* (*NATO-ASI Series C* vol C529) ed C Caccomo *et al* (Dordrecht: Kluwer) p 197
[40] Binder K and Ciccotti G (ed) 1996 *Monte Carlo and Molecular Dynamics of Condensed Matter Systems* (Bologna: Soc. Italiana di Fisica)
[41] Yaneva J, Milchev A and Binder K 2004 *J. Chem. Phys.* **121** 12632
[42] Binder K (ed) 1995 *Monte Carlo and Molecular Dynamics Simulations in Polymer Science* (New York: Oxford University Press)
[43] Binder K and Milchev A 2000 *J. Comput.-Aided Mater. Des.* **9** 33
[44] Bennemann C, Binder K and Dünweg B 1998 *Phys. Rev.* E **57** 843
[45] Paul W, Baschnagel J, Bennemann C and Binder K 1999 *J. Phys.: Condens. Matter* **11** 2179
[46] Müller M and Gonzalez MacDowell L 2000 *Macromolecules* **33** 3902
[47] Milchev A and Binder K 2001 *J. Chem. Phys.* **114** 8610
[48] Milchev A I and Milchev A A 2001 *Europhys. Lett.* **56** 695
[49] Debrégeas G, Martin P and Brochard-Wyart F 1995 *Phys. Rev. Lett.* **75** 3886
[50] Milchev A and Binder K 1997 *J. Chem. Phys.* **106** 1978
[51] Dutcher J, Dalnoki-Veress K, Nickel B and Roth C 2000 *Macromol. Symp.* **159** 143
[52] Milchev A and Binder K 2002 *J. Chem. Phys.* **116** 7691
[53] Yaneva J, Milchev A and Binder K 2003 *Macromol. Theory Simul.* **12** 573
[54] Doi M and Edwards S F 1986 *The Theory of Polymer Dynamics* (Oxford: Clarendon)